# Temporal Changes in Aqu/C-60 Physical-Chemical, Deposition, and Transport Characteristics in Aqueous Systems

**ARTICLE** *in* ENVIRONMENTAL SCIENCE & TECHNOLOGY · JUNE 2011

Impact Factor: 5.33 · DOI: 10.1021/es1041145 · Source: PubMed



**5 AUTHORS**, INCLUDING:

Cissy Ma

United States Environmental Protection Age…

**22** PUBLICATIONS **280** CITATIONS

SEE PROFILE

Environmental Science & Technology

ARTICLE

pubs.acs.org/est

# Temporal Changes in Aqu/$C_{60}$ Physical−Chemical, Deposition, and Transport Characteristics in Aqueous Systems

Carl Isaacson,[†] Wei Zhang,[†] Tremaine Powell,[†] Xin Ma,[‡] and Dermont Bouchard*[,†]

[†]National Exposure Research Laboratory, Office of Research and Development, U.S. EPA, Athens, Georgia, United States

[‡]National Risk Management Research Laboratory, Office of Research and Development, U.S. EPA, Cincinnati, Ohio, United States

Supporting Information

**ABSTRACT:** Little is known about how temporal changes in the physical−chemical properties of $C_{60}$ aggregates formed in aqueous systems (termed aqu/$C_{60}$) can impact transport pathways contributing to ecological exposures. In this study three aqu/$C_{60}$ suspensions of short-term (100 days), intermediate-term (300 days), and long-term (1000 days) water exposure were first characterized for particle size distribution, water/toluene phase distribution, and surface chemistry. Then, aqu/$C_{60}$ deposition to a model silica surface and transport in porous media were studied by quartz crystal microbalance (QCM) and saturated sand columns. As suspension time increased, aqu/$C_{60}$ particle size shifted to a larger size range as determined by asymmetric flow field-flow fractionation (AF4) and the aqu/$C_{60}$ distribution to toluene was reduced, likely due to surface polarization as revealed by nuclear magnetic resonance (NMR) and UV−visible spectroscopy of the aqu/$C_{60}$ suspensions. Additionally, the deposition to silica surfaces in both QCM and column studies decreased with increased water exposure time. Although a small increase in aqu/$C_{60}$ aggregate size with time may partially explain the greater transport of the long-term aqu/$C_{60}$ because of the decreased collector efficiency for larger submicrometer particles, the polarization of the aqu/$C_{60}$ (thus a more hydrophilic surface) revealed by the toluene/water phase distribution and confirmed by NMR, is considered the determining factor.

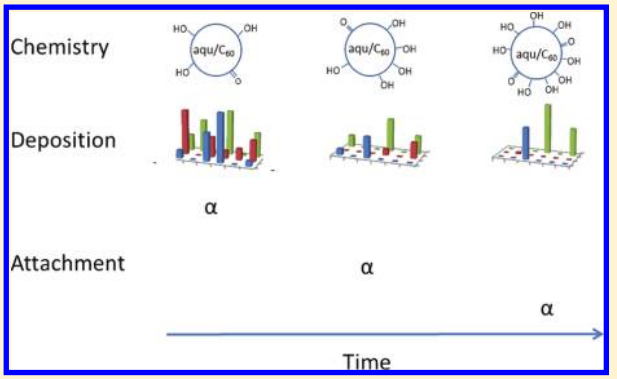


## INTRODUCTION

The industrial manufacture of fullerenes for nanotechnology applications is growing, with close to 1000 consumer products on the market that claim to contain nanoscale materials.[1] Uses of fullerenes and other carbon-based nanomaterials in consumer products are second only to those of nanosilver.[1] With rising production levels it is expected that environmental fullerene levels will increase,[2,3] and the subsequent potential for human and ecological exposures underscores the importance of understanding the basic physical−chemical properties that control the long-term transport and fate of fullerenes in environmental systems.[4]

Though the estimated water solubility of $C_{60}$ fullerene is very low ($1.11 \times 10^{-11}$ M),[5] $C_{60}$ is readily suspended in water to form nanometer-sized aggregates at concentrations several orders of magnitude greater than its water solubility.[6−9] Recent studies have indicated that aqu/$C_{60}$ may persist in the aqueous phase for up to several months[6,8−11] and this dispersal is enhanced by sunlight and humic acid.[8,12] Furthermore, the phase distribution of $C_{60}$ aggregates formed in aqueous systems (termed aqu/$C_{60}$) to toluene may decrease as the aqu/$C_{60}$ suspensions age,[9,13] indicating possible changes in the surface chemistry of aqu/$C_{60}$ aggregates. If aqu/$C_{60}$ surface properties, and subsequently phase distribution behavior, are dynamic qualities, then the kinetics of aqu/$C_{60}$ surface characteristics and interactions with environmental matrices must be considered when assessing aqu/$C_{60}$ transport, fate, and bioaccumulation in environmental systems. Nonetheless, only short-term suspensions (i.e., less than 5 months)[11] have been used in previous studies, thus the properties of the long-term aqu/$C_{60}$ remain elusive.

The objectives of this study were to explore the changes in aqu/$C_{60}$ physical−chemical characteristics, deposition, and transport in porous media over the course of a 3-year period. To achieve these objectives a new analytical method (termed phase dissolution) was developed to quantify the concentration of aqu/$C_{60}$. Changes in aqu/$C_{60}$ particle size and mass distributions were measured using asymmetric-flow field flow fractionation (AF4) coupled with in-line dynamic light scattering (DLS) and liquid-chromatography atmospheric pressure photoionization mass spectrometry (LC-APPI-MS). Quartz crystal microbalance (QCM) deposition studies were conducted to assess changes in aqu/$C_{60}$ deposition onto silica surfaces. Finally, 1-dimensional column transport studies, that integrated multiple

**Received:** December 8, 2010
**Accepted:** May 4, 2011
**Revised:** April 29, 2011
**Published:** May 17, 2011

Table 1. Key Properties of Aqu/$C_{60}$ Colloidal Suspensions in 10 mM Buffer Solutions Over a 3-Year Period[a]

| treatment | | duration (days) | pH | $D_h$ (nm) | PDI | EM ($\mu$m cm/(sV)) | $\zeta$-potential (mV)[b] | concentration ($\mu$g/L) PD | concentration ($\mu$g/L) L:L | PD/L:L ratio |
|---|---|---|---|---|---|---|---|---|---|---|
| short-term suspension | no. 1 | 99 | 7.77 | 165 ± 2 | 0.202 | −3.90 ± 0.31 | −49.8 ± 4.0 | 151 ± 12 | 106 ± 2 | 1.4 |
| | no. 2 | 115 | 7.85 | 171 ± 2 | 0.163 | −3.74 ± 0.21 | −47.6 ± 2.7 | 179 ± 11 | 102 ± 18 | 1.8 |
| intermediate-term | no. 1 | 304 | 7.85 | 177 ± 2 | 0.177 | −3.52 ± 0.12 | −44.9 ± 1.5 | 126 ± 45 | 77 ± 18 | 1.6 |
| suspension | no. 2 | 309 | n/a | 168 ± 2 | 0.134 | −4.14 ± 0.20 | −52.8 ± 2.5 | 244 ± 52 | 119 ± 41 | 2.0 |
| long-term suspension | no. 1 | 1051 | 7.91 | 169 ± 2 | 0.191 | −4.05 ± 0.44 | −51.6 ± 5.6 | 161 ± 17 | 9 ± 2 | 18 |
| | no. 2 | 1059 | 7.96 | 172 ± 1 | 0.168 | −4.08 ± 0.15 | −52.0 ± 1.9 | 132 ± 22 | 14 ± 1 | 10 |
| | no. 3 | 1075 | 7.87 | 175 ± 1 | 0.163 | −3.95 ± 0.17 | −50.4 ± 2.2 | n/a | n/a | n/a |

[a] Aqu/$C_{60}$ suspensions were buffered in 0.4 mM $NaHCO_3$ and 9.6 mM NaCl solution (i.e., total of 10 mM $Na^+$) and refiltered. $D_h$ is hydrodynamic diameter, EM is electrophoretic mobility, PD is the phase dissolution method, L:L is the liquid:liquid extraction method, and the reported values are means and 95% confidence limits from three to six replicated measurements. [b] $\zeta$-potential values were calculated from the EM values using the Smoluchowski equation.

retention mechanisms, were conducted using saturated sand columns. Since it has been shown that the method of $C_{60}$ suspension preparation may significantly affect $C_{60}$ aggregate properties including particle size and surface charge,[14,15] this study utilized an extended mixing with water protocol that is more representative of the processes likely to act on $C_{60}$ following its release into the environment. This study addresses the data gap in the current literature on how the phase distribution, deposition, and transport behaviors of aqu/$C_{60}$ change as the time of exposure to water progresses.

## MATERIAL AND METHODS

**Generation of Aqu/$C_{60}$ Suspensions.** The bulk aqu/$C_{60}$ suspensions were prepared by stirring in deionized water as previously described.[6,11] Briefly, 100 mg of $C_{60}$ powder was added to 400 mL of deionized water (18 MΩ/cm) and then stirred on magnetic stir plates under ambient laboratory lighting. As aqu/$C_{60}$ has antimicrobial properties,[15] other than using 0.22 $\mu$m-filtered deionized water and clean glassware no further steps were taken to limit microbial growth. Microbial growth in the bulk aqu/$C_{60}$ suspensions would be unlikely, because of the antimicrobial activity of aqu/$C_{60}$, the lack of nutrients required for microbial growth, and the nonbiodegradability of $C_{60}$.[16] Subsamples of aqu/$C_{60}$ suspensions were collected from three different suspensions that were stirred for approximately 99, 309, and 1075 days (i.e., short, intermediate, and long intervals) (Table 1). Before sampling, the mixtures were allowed to free-settle for 24 h and then a 20-mL aliquot was collected 2 cm below the suspension surface. Prior to all characterization, deposition, and transport studies the aqu/$C_{60}$ aliquots were filtered through a prewashed 0.45-$\mu$m cellulose acetate filter. During these studies each suspension was monitored for changes in size and $\zeta$-potential and no changes were observed. Using this sampling and filtration technique, filter ripening and associated aqu/$C_{60}$ filter retention were minimized as determined by visual inspection of the filters and instrumental quantification of the filtrate. The mass of aqu/$C_{60}$ lost during filtration was not measured, as the fraction of aqu/$C_{60}$ able to pass through a 0.45-$\mu$m filter is of greater interest in aqueous environmental transport and toxicology studies than the fraction retained by 0.45-$\mu$m filter and subsequently is the focus of this work. For the QCM and column transport studies, which required larger sample volumes, multiple aliquots were collected as described and combined (i.e., 100 mL). Then the solution chemistry of the filtered aliquots was adjusted with 0.4 mM $NaHCO_3$ and 9.6 mM NaCl so that the solution pH was 7.8 and ionic strength was 10 mM. After an overnight equilibration period, these aliquots were filtered again prior to use.

**Determination of Aqu/$C_{60}$ Mass, Size, Charge, and Surface Chemistry.** Quantification of aqu/$C_{60}$ mass suspended in water was achieved by two methods: liquid−liquid extraction to toluene with salting-out by sodium chloride, or by dissolution of the aqueous suspension into a mixture of toluene and methanol, referred to here after as "phase dissolution". Additional information on the quantification methods and phase dissolution method development is provided in Supporting Information. For both methods, the $C_{60}$ concentration in the toluene phase was quantified by LC-APPI-MS as described previously.[8,17]

All $^{13}C$ NMR spectra were recorded on a Varian Inova 600 MHz spectrometer at 20 °C with a 5-mm broadband probe (Varian, Palo Alto, CA). Aqu/$C_{60}$ suspension samples were prepared by stirring 3.1 mg of 20−30% $^{13}C$ enriched $C_{60}$ (MER Corp., Tucson, AZ) in 10 mL of deionized water containing 10% $^2H_2O$. A description of NMR spectra collection and analysis is available in Supporting Information.

For characterization of aqu/$C_{60}$ suspensions, the UV/Visible light absorbance was recorded from 200 to 800 nm using a UV/Visible spectrometer (Lambda 35 spectrophotometer, PerkinElmer, Waltham, MA). A description of UV/Visible calibration for column tests is available in the Supporting Information.

Size and $\zeta$-potential measurements were made by dynamic light scattering (DLS) in batch mode on a Malvern Zetasizer NanoZS (Malvern, Westborough, MA). For measurements of $\zeta$-potential the instrument uses phase angle light scattering to measure the electrophoretic mobility (EM) of aqu/$C_{60}$ aggregates. Six measurements, consisting of 12 runs each, were acquired for each sample. The $\zeta$-potential of aqu/$C_{60}$ aggregates was calculated from the EM values using the Smoluchowski equation. For aggregate size determinations DLS correlates fluctuations in photons scattered by particles with time. The diffusion coefficient is calculated from this correlation by the cumulant method. The intensity-weighted hydrodynamic size distribution, $D_h$, is then calculated from the diffusion coefficient via the Stokes−Einstein equation. The $D_h$ is a single, intensity-weighed value representing the entire aggregate size distribution. Each reported $D_h$ is the average of six measurements consisting of 12 runs.

**Table 2. Column Experiment Properties and Modeled Transport Parameters[a]**

| experimental sets | | measured parameters | | | modeled parameters | | |
|---|---|---|---|---|---|---|---|
| treatments | tests | Θ | $v$ (cm/min) | $M_{ER}$ | $D$ (cm$^2$/min) | $k_d$ (min$^{-1}$) | $R^2$ |
| tracer $^3H_2O$ | 1 | 0.45 | 0.30 | 0.99 | 0.017 | 0 | 0.995 |
| | 2 | 0.43 | 0.30 | 1.01 | 0.010 | 0 | 0.978 |
| | 3 | 0.44 | 0.29 | 0.98 | 0.006 | 0 | 0.998 |
| | mean | 0.44 | 0.30 | 0.99 | 0.011 | 0 | |
| short-term aqu/$C_{60}$ | 1 | 0.44 | 0.30 | 0.72 | 0.011 | 0.015 | 0.979 |
| | 2 | 0.44 | 0.30 | 0.80 | 0.011 | 0.011 | 0.958 |
| | 3 | 0.44 | 0.30 | 0.82 | 0.011 | 0.010 | 0.974 |
| | mean | 0.44 | 0.30 | 0.78 | | 0.012 | |
| intermediate-term aqu/$C_{60}$ | 1 | 0.44 | 0.30 | 0.81 | 0.011 | 0.010 | 0.991 |
| | 2 | 0.44 | 0.30 | 0.66 | 0.011 | 0.019 | 0.990 |
| | 3 | 0.44 | 0.30 | 0.82 | 0.011 | 0.009 | 0.995 |
| | 4 | 0.44 | 0.30 | 0.87 | 0.011 | 0.007 | 0.995 |
| | mean | 0.44 | 0.30 | 0.79 | | 0.011 | |
| long-term aqu/$C_{60}$ | 1 | 0.43 | 0.30 | 0.92 | 0.011 | 0.004 | 0.994 |
| | 2 | 0.44 | 0.30 | 0.93 | 0.011 | 0.003 | 0.995 |
| | 3 | 0.44 | 0.30 | 0.97 | 0.011 | 0.002 | 0.994 |
| | mean | 0.44 | 0.30 | 0.94 | | 0.003 | |

[a] $\theta$ = column porosity, $v$ = average pore water velocity, $M_{ER}$ = effluent mass recovery of input pulse, $D$ = hydrodynamic dispersion coefficient, $k_d$ = deposition rate coefficient.

In addition to particle size determination by batch DLS, aqu/$C_{60}$ suspensions were fractionated with asymmetric flow field flow fractionation (AF4) coupled with in-line DLS, as described previously.[8,17] The aqu/$C_{60}$ were prepared and fractionated in deionized water as deposition on the AF4 membrane did not permit fractionation in 10-mM $Na^+$ solutions. The AF4 (Postnova, Salt Lake City, UT) was outfitted with a 10-kDa PES membrane, a 0.5-mL injection loop, and deionized water eluent. The eluent from the AF4 was passed through a DLS instrument in flow-through mode. The DLS correlates the fluctuations in scattered light with time as described above, however in flow-through mode the instrument records a single $D_h$ average representing the size over a 3-s increment. Fractions were collected every 2 min from the AF4 for quantification by phase dissolution and LC-APPI-MS.

**Aqu/$C_{60}$ Deposition Studies with Quartz Crystal Microbalance (QCM).** A quartz crystal microbalance with dissipation monitoring (QCM-D) (E4, Q-sense, Västra Frölunda, Sweden) was used to monitor the deposition of aqu/$C_{60}$ on a model surface. The crystals used for the QCM-D studies were AT-cut quartz sensor crystals with a silica-coated ($SiO_2$) surface (QSX-303, Qsense). For all experiments, the chamber temperature was 25.0 °C and the flow rate through the measurement chamber was 0.1 mL/min. According to the manufacturer, this flow rate results in a laminar flow across the sensor, and minimizes the development of air bubbles.

For each deposition experiment, the background electrolyte solution (0.4 mM $NaHCO_3$ and 9.6 mM NaCl, pH 7.8, total of 10 mM $Na^+$) was first flowed across the surface of the crystal until the normalized third overtone frequency monitored by the QCM stabilized; stabilization was achieved when the normalized frequency drifted <0.33 Hz in a 10 min time period. Then the aqu/$C_{60}$ suspensions were passed over the sensor surface for 20 min, followed by a 10 min rinse with the background electrolyte solution. The deposition rate was calculated by taking the slope of the initial frequency change in the presence of aqu/$C_{60}$. Crystals were then removed from the system, and gently dried under $N_2$ gas for AFM imaging.

**Atomic Force Microscopy (AFM) Imaging.** QCM crystals were mounted on a stainless steel AFM mount by placing a small piece of double-sided conductive tape on the mount, then adhering the crystal to the mount. All images were made using a Veeco Multimode AFM with Nanoscope V controller and J-Scanner. Images were produced in "tapping mode" with TESP cantilevers with an image size of 30 um, speed of 0.3 Hz, and a resolution of 512 × 512 pixels. All images were taken near the center of each crystal imaged.

**Column Transport Studies.** Angular high-purity Iota quartz sand (99.9% silicon dioxide, Unimin Corporation, New Canaan, CT) with 16% of the sand between 250 and 300 $\mu$m and 83% of the sand between 125 and 250 $\mu$m was used as a model porous medium. The quartz was sieved to select the particle 125−300 $\mu$m size grains, washed with deionized water, oven-dried, and stored in a closed container prior to use. Pulse breakthrough experiments (3 pore volumes) were conducted to characterize the transport properties of the short-term, intermediate-term, and long-term aqu/$C_{60}$ suspensions in saturated sand under a steady-state pore water velocity ($v$) of 0.30 cm/min (i.e., the flow rate $q$ = 0.233 mL/min and the Darcy velocity $U$ = 190 cm/day). The same background solution used in the studies described above (0.4 mM $NaHCO_3$ and 9.6 mM NaCl, pH 7.8, total of 10 mM $Na^+$) was deaerated prior to use. Triplicate tracer experiments with tritiated water ($^3H_2O$) were conducted to define the hydrodynamic properties of the columns (Table 2). The aqu/$C_{60}$ mass loss in the experimental apparatus was evaluated by conducting the media-free column experiments. The breakthrough curves (BTCs) of aqu/$C_{60}$ suspensions were fitted by a convection−dispersion equation with a kinetic deposition term to estimate the deposition rate coefficient ($k_d$). The attachment efficiency ($\alpha$) of aqu/$C_{60}$ was determined from $k_d$

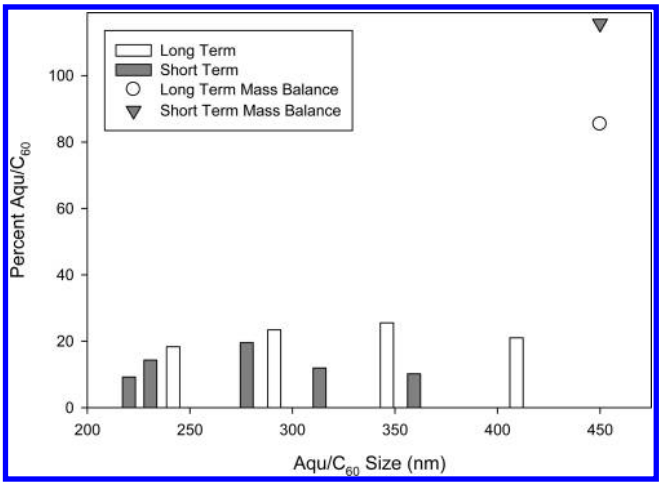


**Figure 1.** AF4-DLS mass and size distributions of short-term and long-term aqu/$C_{60}$ suspensions in deionized $H_2O$. Triangle and circle at far right indicate mass balance achieved in AF4 separation.

after estimating the single-collector contact efficiency ($\eta_0$). Detailed description of column experiments, modeling of BTCs, and calculation of $\eta_0$ and $\alpha$ are provided in the Supporting Information.

## RESULTS AND DISCUSSION

**Aqu/$C_{60}$ Physical−Chemical Characteristics Change with Time.** Aqu/$C_{60}$ suspensions were characterized to determine how aggregate size, $\zeta$-potential, and distribution to a nonpolar phase (toluene) changed from 99 to 1075 days of exposure to water (Table 1). Although the particle size data from batch DLS measurements indicate no trends in $D_h$ or size distribution with time (Table 1 and SI 1), AF4-DLS analyses indicate that the aqu/$C_{60}$ mass distributions of the long-term stirred aqu/$C_{60}$ were shifted to larger sizes compared to the short-term treatments (Figure 1). The long-term aqu/$C_{60}$ ranged in size from 240 to 410 nm in $D_h$, while short-term aqu/$C_{60}$ ranged from 220 to 360 nm in $D_h$ (Figure 1). While this observation seems counterintuitive (particle sizes would be expected to decrease due to shear force as stirring time increases), changes in the surface chemistry of pristine powder $C_{60}$ as $C_{60}$ is transformed into aqu/$C_{60}$ may result in differing particle size distributions. Differences between sizes determined by AF4 in Figure 1 and batch DLS measures in Table 1 may result from the extra filtration steps taken to prepare the aqu/$C_{60}$ in 10 mM $Na^+$ for the transport and deposition studies. Additionally, the sizes determined by AF4-DLS coupled off-line with LC-MS are more informative than DLS batch measurements; as AF4 with inline DLS size separates aqu/$C_{60}$ prior to size measurement with DLS it provides a solution to the problem created by high particle size polydispersity in environmental samples and the occlusion of small particles by larger particles resulting from the $10^6$ dependence of light scattering intensity on particle size. The size distribution reported here (220−410 nm in $D_h$) is significantly larger than we previously reported for aqu/$C_{60}$ generated in deionized water by sonication, 80−250 nm[17] and for sunlight exposed aqu/$C_{60}$, 140−230 nm.[8] These results indicate that if a larger amount of energy is input to the system, through sonication or exposure to sunlight, smaller aggregates will be generated. Additionally, the time of exposure to water as well as electrostatic,

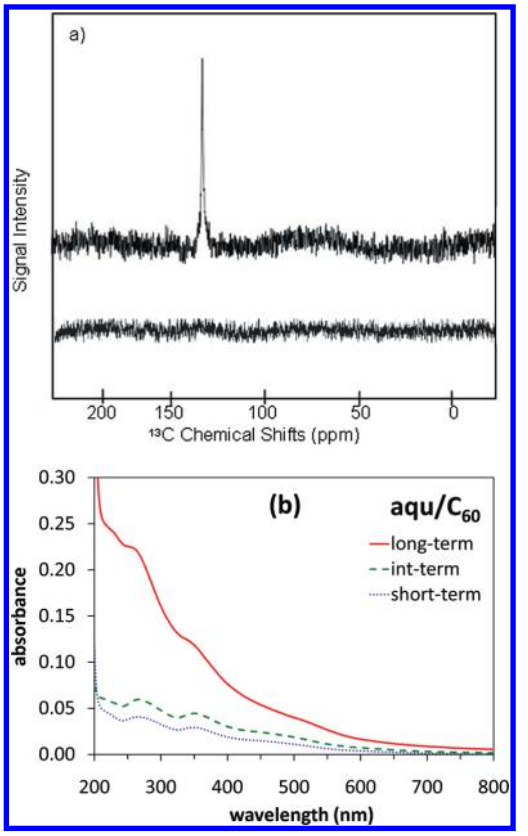


**Figure 2.** (a) NMR spectra of 3-month stirred $^{13}C_{60}$ enriched aqu/$C_{60}$ suspension (top trace) showing peak at 143 ppm and 2-year stirred (bottom trace) showing no peak at 143 ppm. (b) Ultraviolet/Visible spectrum of the short-term, intermediate-term, and long-term aqu/$C_{60}$ suspensions.

hydrophobic, and other forces controlling aqu/$C_{60}$ interactions may influence aqu/$C_{60}$ size.

As observed by Ma and Bouchard[6] in a 111-day study, the aqu/$C_{60}$ $\zeta$-potential measurements did not change significantly over the 1075-day course of this study; however, changes in the phase distribution characteristics of aqu/$C_{60}$ were observed over the same time period (Table 1). To measure changes in aqu/$C_{60}$ extraction characteristics over time, the phase dissolution method, which solubilizes the whole suspension aliquot in a solution of methanol and toluene, was compared to liquid−liquid extraction which requires aqu/$C_{60}$ redistribution to toluene. The phase dissolution concentration values remain relatively constant through the experimental period (Table 1); however, the long-term liquid−liquid extraction values are about an order of magnitude lower than the liquid−liquid extraction values at the short and intermediate time periods. These differences are clearly reflected in the phase dissolution/liquid−liquid extraction ratios. Pristine $C_{60}$ is hydrophobic. As $C_{60}$ begins to interact with water, it is anticipated to be readily extracted into nonpolar toluene. However, upon exposure of aqu/$C_{60}$ to water for extended time periods, less aqu/$C_{60}$ partitions into toluene phase indicating the hydrophobicity of aqu/$C_{60}$ decreases as aqu/$C_{60}$ becomes hydroxylated upon exposure to water, as proposed by Labille et al.[18] In a shorter-term study Ma and Bouchard[6] also observed changes in aqu/$C_{60}$ extraction to toluene over time, in some cases as early as 100 days.

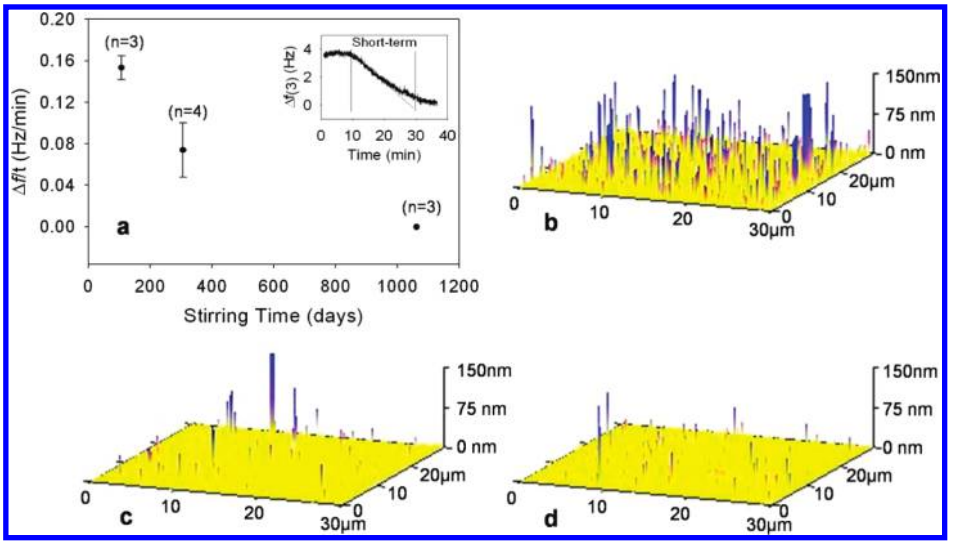


**Figure 3.** (a) Deposition on $SiO_2$ quartz crystal decreased in the order short, intermediate, and long-term stirred aqu/$C_{60}$. Vertical bar at 10 min indicates time at which aqu/$C_{60}$ was flowed over the crystal and vertical bar at 30 min indicates time at which electrolyte solution was flowed over the crystal. Error bars are the standard deviation of replicates, and *n* is the number of replicates. Atomic force microscopy images showing deposition decreased from short (b), to intermediate (c), to long-term stirred (d).

Although mass spectrometry did not indicate the presence of any identifiable covalently bonded aqu/$C_{60}$ transformation products (Figure S2), significant changes were observed in both the $^{13}C$ NMR and UV spectra (Figure 2 a and b). The NMR spectra of a separately prepared 120-day stirred aqu/$C_{60}$ suspension enriched in $^{13}C_{60}$ indicated a single peak at 143 ppm, which is shifted upfield slightly from previous reports;[7] however, 750-day-stirred aqu/$C_{60}$ showed no peak in the region of 143 ppm, indicating that aqu/$C_{60}$ surface had become significantly polarized over time, likely through hydroxylation interactions with water. A similar change in NMR spectra was reported by Hou et al. upon oxidation of aqu/$C_{60}$ when exposed to sunlight.[10]

The aqu/$C_{60}$ UV/Visible spectra showed the typical peaks between 250 and 400 nm wavelengths, similar to that reported previously.[7,12] However, compared to the short-term and intermediate-term aqu/$C_{60}$ suspensions at similar total $C_{60}$ concentrations, the UV/vis spectrum of the long-term aqu/$C_{60}$ suspension had stronger absorbance and much broader peaks (Figure 2 b). Because the concentration of aqu/$C_{60}$ was similar for all treatments, (Table 1), the increased absorbance for the intermediate and long-term stirred aqu/$C_{60}$ may indicate that as aqu/$C_{60}$ becomes increasingly hydroxylated with increased stirring time its UV attenuation coefficient increases. However, the presence of the intrinsic $C_{60}$ absorbance peaks indicate that the cage structure of $C_{60}$ remains intact throughout the 1075 day stirring time. These spectra, as well as the observation that aqu/$C_{60}$ phase distribution to toluene decreased over time, are strong evidence of changes in the surface chemistry of aqu/$C_{60}$ as $C_{60}$−water contact time increases.

**Quartz Crystal Microbalance (QCM) Deposition Studies with Atomic Force Microscopy (AFM) Imaging.** One of the key objectives of this study was to quantify the effects of changes in aqu/$C_{60}$ physical and chemical properties on deposition and transport. QCM deposition measurements indicate that the short-term aqu/$C_{60}$ was readily deposited ($0.90 \pm 0.17$ ng/(min-cm$^2$)) on the $SiO_2$ surface while intermediate-term aqu/$C_{60}$ was less readily deposited ($0.44 \pm 0.25$ ng/(min-cm$^2$)), and no deposition was observed for long-term stirred aqu/$C_{60}$ (Figure 3). Short and intermediate term stirred aqu/$C_{60}$ showed deposition rates similar to those reported by Chen and Elimelech;[19,20] however, for the long-term stirred aqu/$C_{60}$ the deposition rates were significantly lower than those reported by Chen and Elimelech. The lower deposition rates for the long-term stirred aqu/$C_{60}$ likely result from the formation hydroxylated aqu/$C_{60}$ at longer stirring times resulting in less hydrophobic aggregates and less deposition. To confirm that the observed frequency shift was caused by particle deposition, the frequency shift of the crystal was measured in background electrolyte solution where no frequency change was observed (Figure 3). These results indicate that as aqu/$C_{60}$ is stirred in water it becomes more stable in suspension and less readily deposited on surfaces.

To visualize and measure the size of the aqu/$C_{60}$ deposited on the QCM crystals, AFM images were collected of the crystal surface (Figure 3b−d). The AFM images corroborate the QCM measurements of decreasing deposition as $C_{60}$-water contact time increased (Figure 3b−d). Additionally, the aqu/$C_{60}$ deposited on the QCM crystal surface showed no size trends in the deposited aggregates across treatments with most of the deposited aggregates being less than 150 nm (Figure 3b−d). The small size of the deposited aqu/$C_{60}$ indicates that only a fraction of the aqu/$C_{60}$ is readily deposited, since greater than 85% of the mass of aqu/$C_{60}$ has a $D_h$ between 220 and 410 nm as determined by AF4-DLS with quantification by mass spectrometry (Figure 1). The lack of aqu/$C_{60}$ aggregates with a $D_h$ less than 150 nm in the AF4-DLS results may arise from loss of smaller aqu/$C_{60}$ particles during AF4 separation and from lower DLS sensitivity for smaller particles. Selective deposition of the smallest aggregates is consistent with classic filtration theory which states that smaller particles have a greater propensity to be deposited, greater collector efficiency, due to their larger diffusion coefficient.[21,22] However, differences in aggregate size do not fully describe the differences in deposition among the different time-course treatments. The increased surface polarity of aqu/$C_{60}$ is likely a much greater contributor to the decreased deposition of the long-term stirred aqu/$C_{60}$.[23,24]

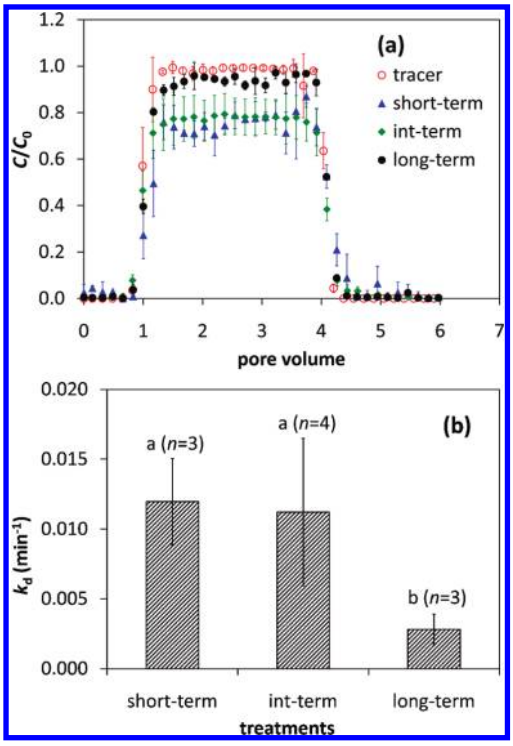


**Figure 4.** Mean breakthrough curves (BTCs) of the $^3H_2O$ tracer and aqu/$C_{60}$ suspensions (a) and estimated deposition rate coefficient ($k_d$) in saturated sand columns. Error bar is the standard deviation of replicates, and $n$ is the number of the replicates. Means of $k_d$ with different lower case letters are significantly different ($P < 0.05$, two-tails) by the least significant difference (LSD) method in PASW Statistics 18 (SPSS, Inc., Chicago, IL).

**Column Transport Studies.** The transport of aqu/$C_{60}$ suspensions through saturated sand columns behaved similarly to the conservative tracer with no size-exclusion or retardation effect (Figure 4a). Therefore, it is likely that the aqu/$C_{60}$ aggregates and the tracer sampled the same soil pore space. The absence of a retardation effect suggests that under steady-state conditions the observed retention of the aqu/$C_{60}$ resulted from the irreversible kinetic deposition, and not the equilibrium adsorption that would otherwise delay the breakthrough of the input pulse. The measurable, albeit relatively small, retention of the aqu/$C_{60}$ (Table 2 and Figure 4) is less intuitive because of the formidable primary energy barrier calculated by Derjaguin–Landau–Verwey–Overbeek theory, as a result of the highly negative qζ-potentials of the aqu/$C_{60}$ and quartz. However, the good agreement between theoretical attachment efficiencies at the secondary minima ($\alpha = 0.009$[25]) and the experimental results, 0.003–0.014 (see below), suggests that aqu/$C_{60}$ retention is primarily through deposition in the secondary minima. Additionally, retention from chemical heterogeneities is not likely to be significant because of the high purity of the Iota quartz, and physical straining is likely low because of the low aqu/$C_{60}$ to sand grain diameter ratio (0.00085).[26] However, retention due to surface roughness and hydrodynamic traps at zones of flow stagnation, low flow vortices, and backward flow cannot be discounted.[26,27]

All three aqu/$C_{60}$ suspensions were poorly retained in the saturated sand columns as the average mass recovered in the effluent ranged from 78 to 94% (Table 2), indicating the aqu/$C_{60}$ has the potential to travel significant distances upon entering into groundwater aquifers or river sediments. For a pore groundwater velocity of 0.30 cm/min (i.e., Darcy velocity of 190 cm/day for a porosity of 0.44), the short-term and intermediate-term $C_{60}$ must travel about 1.8 m to achieve a 3-log concentration reduction, whereas the long-term $C_{60}$ would have to travel 6.9 m to achieve 3-log concentration reduction. Following the method of Tufenkji and Elimelech,[22] the attachment efficiency ($\alpha$) of the aqu/$C_{60}$ suspensions was calculated to be 0.014 for the short-term aqu/$C_{60}$, 0.013 for the intermediate-term aqu/$C_{60}$, and 0.003 for the long-term aqu/$C_{60}$, assuming the average particle size of 170 nm, particle density of 1.41 g/cm$^3$,[28] and aqu/$C_{60}$–quartz Hamaker constant of $2.59 \times 10^{-21}$ J.[13] The calculated attachment efficiencies of the short-term and intermediate-term aqu/$C_{60}$ to high purity Iota quartz were similar to that of n-$C_{60}$ generated by the solvent exchange method in thoroughly cleaned glass beads[29] or a Lula soil,[30] but 1 order of magnitude smaller than that of solvent-exchange n-$C_{60}$ in moderately cleaned glass beads[24,28] or natural sand[25,31] under comparable experimental conditions. These comparisons suggest that the aqu/$C_{60}$ transport behavior may vary significantly in different porous media. Additionally, since 5–8% of the aqu/$C_{60}$ was observed to be deposited in the experimental apparatus during media free experiments, the 6% of the aqu/$C_{60}$ retained for the long-term stirred may simply be due to deposition in the experimental apparatus (Table 2).

The observed increase in aqu/$C_{60}$ mobility with extended $C_{60}$–water contact time (Table 2 and Figure 4) may have resulted from several mechanisms, including the change in aqu/$C_{60}$ size distribution quantified with the AF4-DLS measurements, or the increased polarization indicated by the spectral data and decreased hydrophobicity indicated by the toluene distribution data. Our previous studies showed that the ζ-potentials of the aqu/$C_{60}$ were fairly constant after exposure to water for an extended time,[6] which were confirmed with this study as the ζ-potential of the three aqu/$C_{60}$ suspensions were similar (Table 1, Table S1). The relatively constant ζ-potential indicates that the increased mobility is not likely to be of electrostatic origin. However, as demonstrated by AF4-DLS measurement, the short-term suspensions have greater mass in smaller size class (Figure 1). For submicrometer particles, the smaller the particle size is, the greater the chance that the particle will collide with the collector (collector efficiency) due to increased diffusion for the smaller particle according to the classic filtration theory.[21,22] This increased collector efficiency may partially contribute to the greater retention of the short-term suspensions, but would not be the sole factor. Rather, the short-term and intermediate-term aqu/$C_{60}$ suspensions are more likely to be distributed into the nonpolar toluene phase than the long-term aqu/$C_{60}$ as seen in the extractability of $C_{60}$ in Table 1.[9] Therefore, it is more likely that the increase of mobility with $C_{60}$-water contact time resulted from the enhanced hydrophilicity of the aqu/$C_{60}$.

## ■ ENVIRONMENTAL IMPLICATIONS

Estimating fullerene transport and fate in the environment is made problematic by the dynamic nature of aqu/fullerene surface chemistry. Our results clearly indicate that analytical measurements using the popular toluene extraction technique are confounded by temporal changes in aqu/$C_{60}$ extractability. One result of this effect is an underestimation of actual aqu/$C_{60}$ environmental concentrations due to lowered extraction efficiencies

at longer fullerene−water contact times. Changes in aqu/$C_{60}$ surface chemistry will also affect particle−particle and particle−surface interactions, likely resulting in increased suspension stability and decreased deposition on environmental surfaces. This emphasizes that environmental media such as water with which the nanoparticles interact could significantly influence the particle surface chemistry and consequently affect the fate and transport profiles in environmental systems.

## ■ ASSOCIATED CONTENT

**Supporting Information.** Information describing the development of the phase dissolution method, aqu/$C_{60}$ suspension physical−chemical characteristics, aqu/$C_{60}$ mass spectra, AFM characterization of deposition, UV calibration curve and column transport tests is available free of charge via the Internet at http://pubs.acs.org.

## ■ AUTHOR INFORMATION

**Corresponding Author**
*Phone: 706-355-8333; fax: 706-355-8160; e-mail: Bouchard.Dermont@EPA.gov.

## ■ ACKNOWLEDGMENT

We acknowledge Jean-Luc Brousseau (Malvern Instruments), Soheyl Tadjiki (Postnova Analytics), Susan Richardson, U-sa Rattanaudompol, Biplab Mukherjee, Tantiana Burns, and Quincy Teng at EPA Athens for the support provided for this study. This paper has been reviewed in accordance with the U.S. Environmental Protection Agency's peer and administrative review policies and approved for publication. Mention of trade names or commercial products does not constitute endorsement or recommendation for use.

## ■ REFERENCES

(1) Woodrow Wilson International Center for Scholars. *Project on emerging nanotechnologies*. http://www.nanotechproject.org/44. 2007.

(2) Murayama, H.; Tomonoh, S.; Alford, J. M.; Karpuk, M. E. Fullerene Production in Tons and More: From Science to Industry. *Fullerenes, Nanotubes, Carbon Nanostruct.* **2005**, *12* (1 & 2), 1–9.

(3) Wiesner, M. R.; Lowry, G. V.; Jones, K. L.; Hochella, M. F. J.; Di Giulio, R. T.; Casman, E.; Bernhardt, E. S. Decreasing uncertainties in assessing environmental exposure, risk, and ecological implications of nanomaterials. *Environ. Sci. Technol.* **2009**, *43* (17), 6458–6462.

(4) U.S.Environmental Protection Agency. *U.S. Environmental Protection Agency Nanotechnology White Paper*, 2007.

(5) Jafvert, C. T.; Kulkarni, P. P. Buckminsterfullerene's ($C_{60}$) octanol-water partition coefficient ($K_{ow}$) and aqueous solubility. *Environ. Sci. Technol.* **2008**, *42* (16), 5945–5950.

(6) Ma, X.; Bouchard, D. Formation of aqueous suspensions of fullerenes. *Environ. Sci. Technol.* **2009**, *43* (2), 330–336.

(7) Fortner, J. D.; Lyon, D. Y.; Sayes, C. M.; Boyd, A. M.; Falkner, J. C.; Hotze, E. M.; Alemany, L. B.; Tao, Y. J.; Guo, W.; Ausman, K. D.; Colvin, V. L.; Hughes, J. B. $C_{60}$ in water: Nanocrystal formation and microbial response. *Environ. Sci. Technol.* **2005**, *39* (11), 4307–4316.

(8) Isaacson, C. W.; Bouchard, D. C. Effects of humic acid and sunlight on the generation and aggregation state of aqu/$C_{60}$ nanoparticles. *Environ. Sci. Technol.* **2010**, *44* (23), 8971–8976.

(9) Hwang, Y. S.; Li, Q. Characterizing photochemical transformation of aqueous $nC_{60}$ under environmentally relevant conditions. *Environ. Sci. Technol.* **2010**, *44* (8), 3008–3013.

(10) Hou, W.; Kong, L.; Wepasnick, K. A.; Zepp, R. G.; Fairbrother, D. H.; Jafvert, C. T. Photochemistry of aqueous $C_{60}$ clusters: wavelength dependency and product characterization. *Environ. Sci. Technol.* **2010**, *44* (21), 8121−8127.

(11) Bouchard, D.; Ma, X.; Isaacson, C. Colloidal properties of aqueous fullerenes: isoelectric points and aggregation kinetics of $C_{60}$ and $C_{60}$ derivatives. *Environ. Sci. Technol.* **2009**, *43* (17), 6597–6603.

(12) Li, Q.; Xie, B.; Hwang, Y. S.; Xu, Y. Kinetics of $C_{60}$ fullerene dispersion in water enhanced by natural organic matter and sunlight. *Environ. Sci. Technol.* **2009**, *43* (10), 3574–3579.

(13) Ma, X.; Wigington, B.; Bouchard, D. $C_{60}$ Fullerene:surface energy and interfacial interactions in aqueous systems. *Langmuir* **2010**, *26* (14), 11886–11893.

(14) Brant, J. A.; Labille, J.; Bottero, J.-Y.; Wiesner, M. R. Characterizing the impact of preparation method on fullerene cluster structure and chemistry. *Langmuir* **2006**, *22* (8), 3878–3885.

(15) Chae, S.; Badireddy, A. R.; Budarz, J. F.; Lin, S.; Xiao, Y.; Therezien, M.; Wiesner, M. R. Heterogeneities in fullerene nanoparticle aggregates affecting reactivity, bioactivity, and transport. *ACS Nano* **2010**, *4* (9), 5011–5018.

(16) Kümmerer, K.; Menz, J.; Schubert, T.; Thielemans, W. Biodegradability of organic nanoaprticles in the aqueous environment. *Chemosphere* **2011**, *82*, 1387–1392.

(17) Isaacson, C. W.; Bouchard, D. C. Asymmetric flow field flow fractionation (AF4) of aqueous $C_{60}$ colloids with size determination by dynamic light scattering and quantification by liquid chromatography atmospheric pressure photo-ionization mass spectrometry. *J. Chromatogr. A* **2009**, *1217* (9), 1506–1512.

(18) Labille, J.; Masion, A.; Ziarelli, F.; Rose, J.; Brant, J.; Villieras, F.; Pelletier, M.; Borschneck, D.; Wiesner, M. R.; Bottero, J. Y. Hydration and dispersion of $C_{60}$ in aqueous systems: the nature of water-fullerene interactions. *Langmuir* **2009**, *25* (19), 11232–11235.

(19) Chen, K. L.; Elimelech, M. Aggregation and deposition kinetics of fullerene ($C_{60}$) nanoparticles. *Langmuir* **2006**, *22*, 10994–11001.

(20) Chen, K. L.; Elimelech, M. Interaction of fullerene ($C_{60}$) nanoparticles with humic acid and alginate coated silica surfaces: measurements, mechanisms, and enivronmental implications. *Environ. Sci. Technol.* **2008**, *42* (20), 7607–7614.

(21) Yao, K.-M.; Habibian, M. T.; O'Melia, C. R. Water and waste water filtration: Concepts and applications. *Environ. Sci. Technol.* **1971**, *5* (11), 1105–1112.

(22) Tufenkji, N.; Elimelech, M. Correlation equation for predicting single-collector efficiency in physicochemical filtration on saturated porous media. *Environ. Sci. Technol.* **2004**, *38*, 529–536.

(23) Zhuang, J.; Qi, J.; Jin, Y. Retention and transport of amphiphilic colloids under unsaturated flow conditions: Effect of particle size and surface property. *Environ. Sci. Technol.* **2005**, *39* (20), 7853–7859.

(24) Lecoanet, H. F.; Bottero, J.-Y.; Wiesner, M. R. Laboratory assessment of the mobility of nanomaterials in porous media. *Environ. Sci. Technol.* **2004**, *38* (19), 5164–5169.

(25) Li, Y.; Wang, Y.; Pennell, K. D.; Abriola, L. M. Investigation of the transport and deposition of fullerene ($C_{60}$) nanoparticles in quartz sands under varying flow conditions. *Environ. Sci. Technol.* **2008**, *42* (19), 7174–7180.

(26) Li, X.; Li, Z.; Zhang, D. Role of low flow and backward flow zones on colloid transport in pore structures derived from real porous media. *Environ. Sci. Technol.* **2010**, *44* (13), 4936–4942.

(27) Bradford, S. A.; Torkzaban, S. Colloid transport and retention in unsaturated porous media: A review of interface-, collector-, and pore-scale processes and models. *Vadose Zone J.* **2008**, *7* (2), 667–681.

(28) Lecoanet, H. F.; Wiesner, M. R. Velocity effects on fullerene and oxide nanoparticle deposition in porous media. *Environ. Sci. Technol.* **2004**, *38* (16), 4377–4382.

(29) Espinasse, B.; Hotze, E. M.; Wiesner, M. R. Transport and retention of colloidal aggregates of $C_{60}$ in porous media: Effects of organic macromolecules, ionic composition, and preparation method. *Environ. Sci. Technol.* **2007**, *41* (21), 7396–7402.

(30) Cheng, X.; Kan, A. T.; Tomson, M. B. Study of $C_{60}$ transport in porous media and the effect of sorbed $C_{60}$ on naphthalene transport. *J. Mater. Res.* **2005**, *20* (12), 3244–3254.

(31) Wang, Y.; Li, Y.; Fortner, J. D.; Hughes, J. B.; Abriola, L. M.; Pennell, K. D. Transport and retention of nanoscale $C_{60}$ aggregates in water-saturated porous media. *Environ. Sci. Technol.* **2008**, *42* (10), 3588–3594.